INTERNATIONAL JOURNAL OF SATELLITE COMMUNICATIONS
Int. J. Satell. Commun. 2000; **18**:271–291

On signal structures for GNSS-2

Robert Schweikert[1], Thomas Wörz[1,*,†], Riccardo De Gaudenzi[2], Alexander Steingass[3] and Armin Dammann[3]

[1] *AUDENS Advanced Communications Technology Consulting GmbH, P.O. Box 1110, D-82224 Seefeld, Germany*
[2] *European Space Agency, European Space Technology Centre, P.O. Box 299, 2200 AG Noordwijk, The Netherlands*
[3] *Institute for Communications Technology, DLR Research Center Oberpfaffenhofen, P.O. Box 1116, D-82230 Wessling, Germany*

SUMMARY

This paper summarizes the main results of an early investigation on desirable signal structures for the European 'Galileo' civil satellite navigation system. Stemming from the requirements for increased accuracy, reduced time-to-first-fix and integrity information provision, the report describes the logical steps and the related numerical results leading to a novel 'Galileo' signal definition. Although the final parameter definition is largely based on European system constraints, a number of design guidelines like the use of spectrally efficient square-root raised-cosine chip shaping and enhanced data broadcasting are expected to be of general applicability to any future satellite navigation system. Copyright © 2000 John Wiley & Sons, Ltd.

KEY WORDS: GNSS2; Galileo; GPS; global satellite navigation system; signal structure

1. INTRODUCTION

The American Global Positioning System (GPS) originally devised as a military positioning system, has triggered the development of a tremendous amount of civil applications based on positioning and timing services. GPS is rapidly moving toward an enhanced hybrid military/civil system trough the addition to new carriers. The strategic role of satellite-based navigation and time distribution motivated the European authorities to develop its own complementary global navigation satellite system (GNSS). In February 1999, the European Commission officially announced the European initiative, called Galileo [1], and laid out the EC's view on the key features and high-level requirements of the envisaged global satellite-based navigation system (GNSS). Few years before the Galileo communication, the European Space Agency (ESA) initiated preliminary studies to investigate the key aspects of a future GNSS.

* Correspondence to: Thomas Wörz, AUDENS Advanced Communications Technology Consulting GmbH, P.O. Box 1110, D-82224 Seefeld, Germany.
Contract/grant sponsor: ESA; contract/grant number Ref. 12182/96/NL/JSC
† E-mail: thomas.woerz@audens.com

 Accepted October 1999

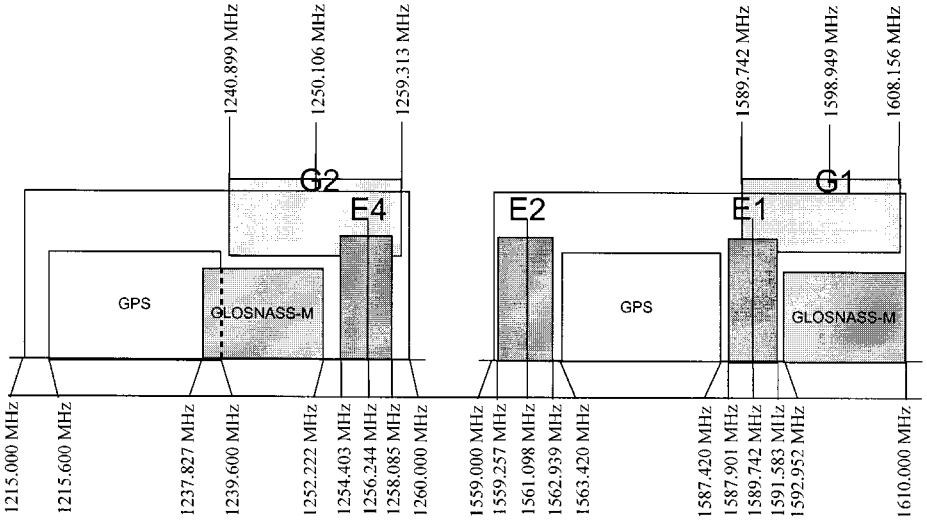

Figure 1. Frequency plan for L-band.

In this contribution, we focus on signal and related system design aspects summarizing the main findings of one of the ESA funded research activity: '*Signal Design and Transmission Performance Study for GNSS-2*' [2]. This study was actually completed before the EC Galileo communication and consequently does not satisfy fully the current system requirements.‡ However, most of its conclusions are still valid and applicable to the on-going Galileo definition.

2. SYSTEM ASSUMPTIONS

For the reasons discussed above, the Signal Design Study was carried-out based on 'educated guesses' about the most likely scenarios. This is particularly true for the Galileo frequency bands whose final allocation is still pending.

2.1. Frequency plan

As "signal baseline" we considered in the study a frequency plan according ESA's 'ENSS' filing which foresees the exploitation of the three L-band frequency slots 'E1', 'E2' and 'E4' (see Figure 1). Although at present, these frequency bands are the most secure for the Galileo system, they exhibit a bandwidth of only about 4 MHz each. Two large bandwidths can be exploited by sharing the GLONASS bands in addition to E1, E4 respectively. In this case, almost 20 MHz of spectrum becomes available in the so-called 'G1', 'G2' bands that jointly with 'E2' constitutes the so-called Option 1. A second option is constituted by the use of potential 30 MHz frequency slot at C-band (5000–5030 MHz) in alternative to E2. Option 2, is the less likely from the regulatory

‡ In particular, the need for a security control access (CAS-2) was not part of the investigation.

Table I. MEO orbit parameters.

Orbital height	20230 km
Orbital plane inclination	55°
Max Doppler shift	4.4–5.2 kHz (L-band) 14.7–17.3 kHz (C-band)
Max number of satellites in view	7–12
Elevation angle	5–90°

standpoint and also because it requires the adoption of a more complex user terminal dual-band RF front-end.

2.2. *Orbital parameters*

According to European Commission Communication [1], a GPS like MEO constellation has been favoured for Galileo. The MEO constellation orbital parameters used for the Signal Design Study have been taken from Parkinson and Spilker [3]. The orbital parameters, used to derive the main system parameters impacting signal design are summarised in Table I.

3. GNSS-2 SIGNAL DESIGN

3.1. *Design drivers*

The main signal design driver has been a target UERE accuracy of the order of 1–2 m[§] with single carrier ranging and 1–2 cm with three carriers differential phase positioning techniques (with the availability of world-wide ionospherical corrections and in the absence of multipath). Furthermore, an increase of the navigation data rate compared with GPS has been envisaged in order reduce the time-to-first-fix (TTFF), and to provide integrity information as well as extended navigation message to users requiring 'enhanced' performance. This may also include broadcast data capabilities for services built on to top of the 'basic' positioning and timing service provided by Galileo. The enhanced data broadcasting capabilities have been achieved with no increase for the satellite Effective Isotropic Radiated Power (EIRP). Because of the large number of expected land-mobile users, attention has been devoted to achieve enhanced signal robustness to the satellite fading channel. The above challenging targets have been achieved, adopting signal design concepts, finding their roots in modern digital wireless CDMA communication techniques.

3.2. *Chip shaping*

3.2.1. Theoretical foundation. For many years Spread Spectrum and CDMA are widely used for military and space applications where emphasis was on anti-jamming and low-power flux density emissions rather than efficient use of the available bandwidth. The recent roll-out of commercial wireless CDMA systems has forced system designers to introduce the apparently controversial

[§]The assumption is pretty much in line with the basic accuracy requirements stated in Reference [1].

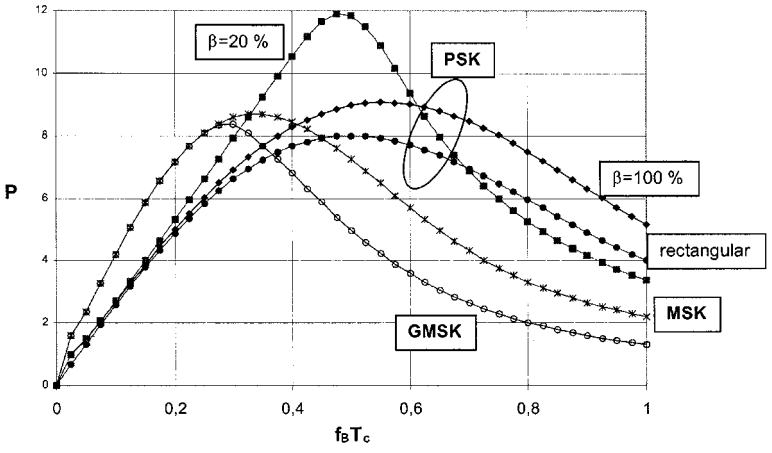

Figure 2. Behaviour of P as a function of $f_B T_c$ for different modulation formats and chip pulse shapes.

concept of *band-limited* Spread Spectrum CDMA systems. Satellite navigation systems can follow a similar path. A well-established view in the navigation community is that rectangular chips are 'a must' to achieve minimum timing measurement jitter for a given C/N_0. The use of rectangular-shaped chips, as in the GPS C/A signal, requires a very large bandwidth compared to the actual chipping rate. Band-limitation of rectangular shaped chips is known to generate sub-optimum chip tracking performance. Communication literature [4] has shown that for a given C/N_0 and chipping rate, DS-SS squared-root raised cosine chip shaping (SRC) provides true signal band-limitation with an actual timing jitter reduction compared to a conventional DS-SS system adopting rectangular chip shaping (REC). Furthermore, SRC band limitation allows a higher chipping rate in the same total bandwidth than near REC chip shaping. This somewhat surprising result found confirmation on an asymptotic analysis based on teh Cramér Rao bound (CRB). Skipping details provided in Reference [2] it can be shown that the CRB for the chip timing jitter is given by

$$\sigma^2_{\mathrm{CRB}} = \frac{B_{\mathrm{L}}}{C/N_0 f_{\mathrm{B}}^2} \frac{1}{P} \tag{1}$$

where B_{L} denotes the bandwidth of the timing loop, f_{B} represents the one-sided available signal bandwidth, and P a function, which depends on the chip pulse shape and modulation format.

Numerical results for the P factor corresponding to REC and SRC PSK, MSK, GMSK are presented in the Figure 2. It clearly appears that SRC chip shaping with small roll-off factor ($\beta = 0.2$) outperforms the other chip modulation formats. The largest value of P (the smallest value of σ^2_{CRB}) clearly is obtained at a normalized bandwidth $f_{\mathrm{B}}\, T_{\mathrm{C}} = 0.5$, i.e. the optimal chipping rate corresponds to the available two-sided bandwidth $2f_{\mathrm{B}}$.

As shown in detail in Reference [4] the SRC DLL steady-state loop jitter dependence on the various parameters is similar to the conventional DLL for REC chips with no bandwidth limitation. However, the conventional jitter expression is multiplied by a constant typically

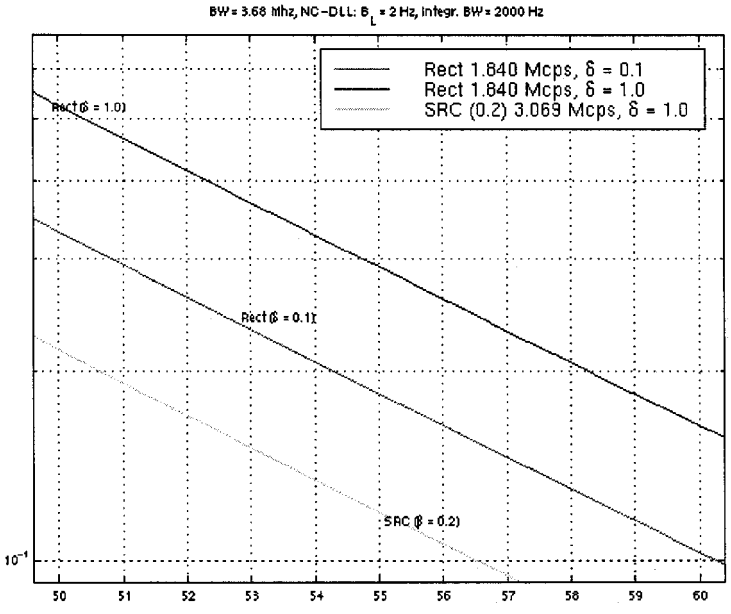

Figure 3. Timing jitter for REC and SRC chip pulse shapes (zoom).

amounts to 0.75. This SRC "corrective" jitter factor implies a saving of about 5 dB in C/N_0 compared to REC.

The claimed advantage of SRC with respect to the REC chip shaping has been further confirmed by the numerical jitter computation in a strictly band-limited channel with a non-coherent Delay Lock Loop (DLL). The example shown in Figure 3, considers the case of an available bandwidth of 3.68 MHz, a DLL loop bandwidth of 2 Hz, and an integration bandwidth of 2000 Hz. For the SRC pulse shaping a roll-off factor of $\beta = 0.2$ is assumed, which leads to a chipping rate of $f_{\mathrm{SRC}} = 3.069$ Mcps. For rectangular-shaped chips it is assumed that the main lobe of the spectrum fits into the available bandwidth, which results in a chip rate of $f_{\mathrm{RECT}} = 1.84$ Mcps. Moreover, for SRC chips, an early-late spacing of $\delta = 1.0\ T_{\mathrm{SRC}}$ (result from Reference [4]), while for REC chips an early-late spacing of $\delta = 1.0\ T_{\mathrm{SRC}}$ (result from Reference [3] and $\delta = 0.1\ T_{\mathrm{RECT}}$ (result from References [5,6]) is chosen.

By comparing the results we can note that the performance of rectangular chips is improved by about 4 dB with a DLL equipped with narrow correlation, although the available two-sided bandwidth is only two times the chip rate. However, the performance of SRC chips is still about 3 dB better due to the higher chip rate possible for SRC shaping in the available bandwidth. No improvement can be expected due to narrow correlation because of the band-limited property of the SRC pulse.

3.2.2. Multipath envelope. The use of higher chipping rates, made possible by SRC chip shaping, provides enhanced resistance to multipath effects for both chip code phase and carrier phase estimation. It is known that multipath negatively affects the chip timing and carrier phase estimate when its relative delay is in the range [0, 1.5* T_{C}]. By increasing $f_{\mathrm{C}} = 1/T_{\mathrm{C}}$ the multipath

sensitive delay window size is reduced proportionally. A code phase estimate error reduction will also diminish line-of-sight carrier phase estimate error induced by multipath.

In the following, the multipath envelopes are computed according to the procedure given in Chapter 14 of Reference [3]. The received signal is composed of the direct component plus a single multipath ray, whose amplitude is multiplied by the factor γ and delayed by δ:

$$r(t) = d(t) + \gamma d(t - \delta). \tag{2}$$

In general, γ is a complex factor with amplitude and phase. For the purpose of determination of the multipath envelope we can restrict the consideration to the real values $\pm\gamma$, which produce the worst cases. The deviation of the nominal tracking point in the loop-S curve of the non-coherent DLL caused by the signal multipath ray as a function of γ and δ has been determined for the above-defined SRC (3.069 Mcps) and REC (1.840 Mcps) chip pulse shapes. The attenuation γ was varied between 0.1 and 0.5 and the delay δ between 0 and 2 μs (= 600 m). Furthermore the early–late spacing of the DLL has been chosen to be $2\Delta = 1$ and 0.1 T_C.

The main conclusions with respect to multipath effects on chip tracking are [2]: (a) As already noted for steady-state jitter, narrow correlation ($2\Delta = 0.1\ T_C$) does not significantly improve the performance of band-limited chip pulse shapes, both SRC and REC. (b) SRC chip pulse provides a lower maximum error and shorter 'main lobe' compared with REC chip pulse, which is due to the higher chip rate. But SRC chip pulse is more sensitive to larger multipath delays, as shown in Figure 4. It is noted that no other loop-S curves resulting from special correlation techniques for multipath suppression, such an MEDLL [5], or (enhanced) strobe correlator [7], have been

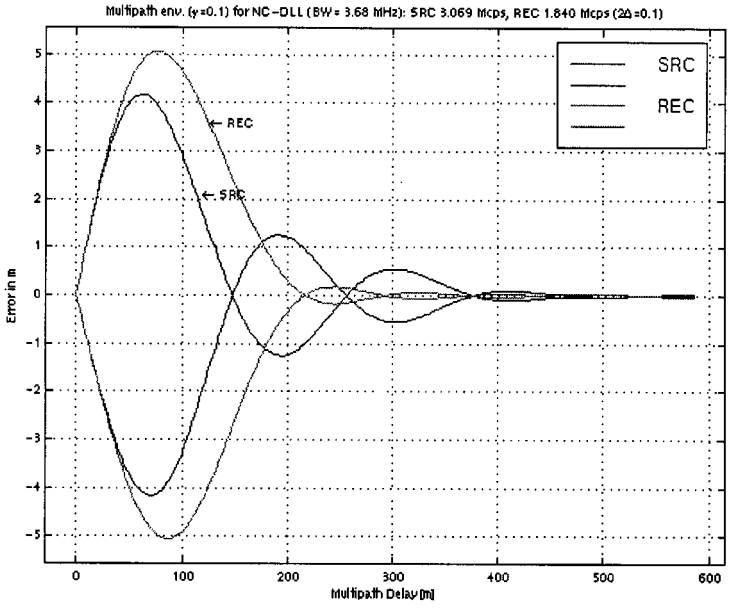

Figure 4. Comparison: SRC pulse shape ($\beta = 0.2$) with a chip rate $f_c = 3.069$ MHz ($2\Delta = 1.0\ T_C$) vs rectangular pulse shape with a chip rate $f_c = 1.840$ MHz ($2\Delta = 0.1\ T_C$).

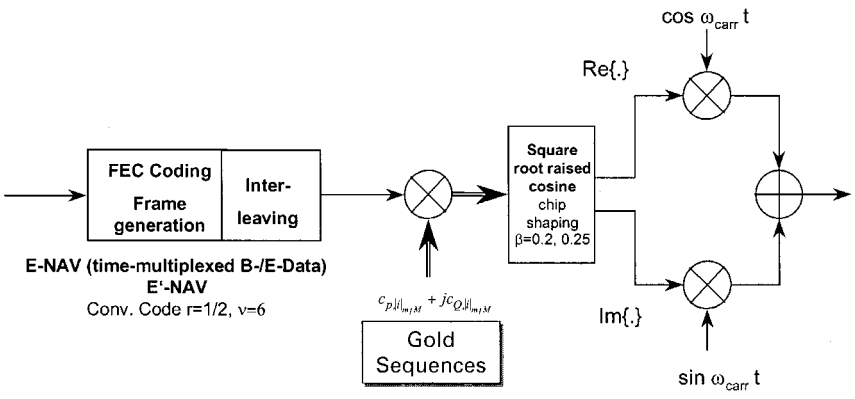

Figure 5. Block diagram of QPN modulation.

considered. But it is anticipated that also for SRC pulse shaping, comparable multipath suppression techniques can be developed.

3.2.3. Receiver implementation advantages. One important SRC-related advantage is that, owing to the signal band-limiting, it is possible to digitally implement the demodulator with a limited number of samples/chip (i.e. 4) with no performance loss. Furthermore, a digital DLL can be efficiently implemented just taking 2 samples/chip after the Chip Matched Filter (CMF). According to modern digital modem design, the 2 samples per chip required for each receiver channel (punctual and early–late) can be readily obtained by linear interpolation of the CMF output samples. In this way the demodulator front-end clock can be completely asynchronous and independent from the incoming signals chip clock.

3.3. Modulator

3.3.1. Signal generation. Figure 5 shows a functional block diagram of the signal generation. The incoming navigation data is organized in frames, encoded with forward error correction (FEC) codes and then time interleaved within one frame. The coded and interleaved navigation data is multiplied with a complex binary spreading chip sequence. Subsequently SRC pulse shaping is applied to the wide-band complex signal, before it is converted to RF band.

The 'complex spreading' provides lower out-of-band emission in presence of a typical non-linear satellite high-power amplifier (HPA). As shown in Figure 6 for two slightly different versions of QPN modulation with SRC chip pulse shaping and a chip rate of 3.069 Mcps, the out-of-band emission at ± 2 MHz is -15 dB for QPN, which is 3 dB less than for BPSK only.

The spreading codes for in- and quadrature phase signal needs to be appropriately chosen in order to minimize the cross-correlation and thus disturbing effects at the receiver. The possibility of using complex data symbols (i.e. 2 bits per symbol) was considered on the one hand for the transmission of a 'pilot' signal, i.e. a known signal in-quadrature for aiding acquisition and carrier phase tracking, and on the other hand for doubling the data rate. The approach with the code division multiplexed 'pilot' signal has not been pursued, since no specific advantage has been

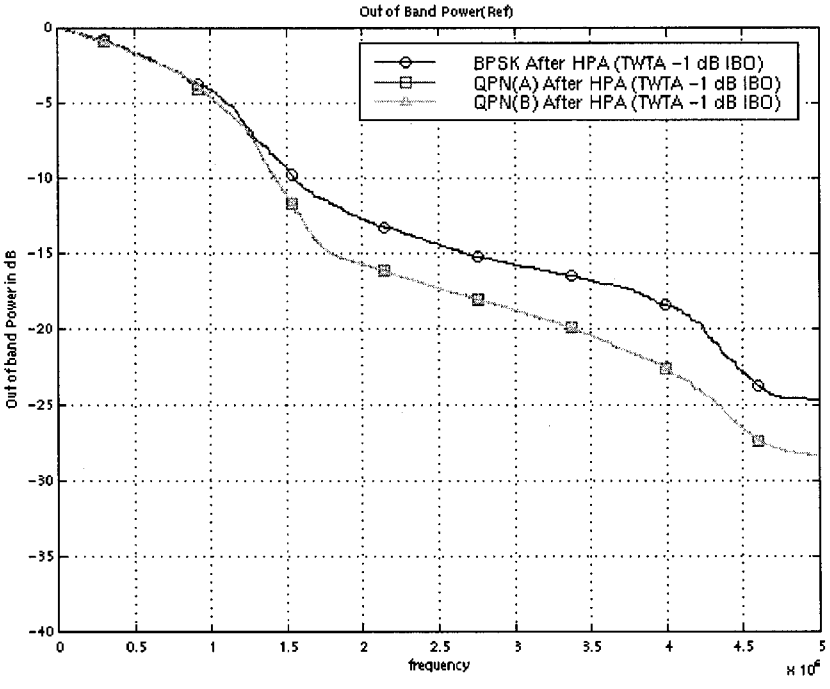

Figure 6. Out-of-band emission versus single-sided bandwidth.

identified for the considered carrier-to-noise-density C/N_0 range from 35 to 45 dB Hz. Furthermore, the in-quadrature pilot will result in a power loss for the useful in-phase BPSK-modulated navigation channel. Doubling the maximum data rate by means of QPSK baseband modulation has also been ruled-out for the resulting robustness of the carrier phase tracking (increased squaring losses and cycle slip rate).

3.3.2. Spreading sequences selection. For PN spreading, gold sequences of length/period $L = 1023$ have been preliminary chosen, mainly since the length of $L = 1023$ fits well all proposed data symbol–chipping rate relationships, Gold codes are known to exhibit good cross-correlation properties, and the choice supports interoperability with GPS. However, the code optimization needs further investigations, in particular, concerning the trade-off between navigation data rate and spreading code sequence length for high chipping rates. Both quantities are strongly interdependent for any given chipping rate, as no data transition is allowed within one spreading code period. Clearly, a longer spreading code word provides a better protection against intra-system interference and narrow-band disturbances, while a higher data rate supports a shorter TTFF and/or the ability for the transmission of additional broadcast data.

3.4. Multiple access: CDMA versus CDMA/FDMA

Designing the system, it needs to be decided, whether, for a given frequency band the total bandwidth (the same centre frequency) is allocated to all satellites (as in GPS) or the available

frequency band is partitioned into M orthogonal frequency slots. By partitioning of the frequency band, the CDMA co-channel interference is decreased resulting is an increased $C/(N_0 + I_0)$, thus, in a reduced standard deviation of the code phase estimation jitter. On the other hand, as the total bandwidth is fixed for the FDMA/CDMA approach, the CDMA processing gain gets smaller, being the chipping rate in each sub-band inversely proportional to M. As a consequence, the standard deviation of the code phase jitter is increased as well. Numerical results [2] computed for various chipping rates clearly indicate that with respect to the ranging accuracy, the CDMA outperforms the FDMA/CDMA approach in the useful range of carrier-to-noise ratios (below about 60 dBHz) considerably.

3.5. Data modulation and coding

Reliable transmission of navigation data, in particular to mobile users, requires the application of certain means to minimise the bit error rate (BER) at the user terminals, such as the application of frame parity bits, forward error correction, interleaving as well as the exploitation of path diversity.[¶] Clearly, no power control techniques are applicable to a one-to-many broadcasting scenario.

The interleaving size is limited by the maximum acceptable modulation/demodulation delay and by frame size constraints. Clearly, for any slow moving user, the gain by interleaving vanishes driving the worst case $E_b/(N_0 + I_0)$ requirement. For our considerations, an interleaving size of one frame, i.e. 1 s has been assumed.

The RMS code phase estimation, chip timing jitter, respectively, can be approximated[‖] by

$$\sigma = cT_c \sqrt{\frac{B_n}{2[C/(N_0 + I_0)]_K} \left(1 + \frac{2W}{[C/(N_0 + I_0)]_K}\right)} \text{(m)} \tag{3}$$

where c is the speed of light, B the non-coherent DLL bandwidth and W the pre-detection bandwidth. The effective carrier-to-noise ratio $C/(N_0 + I_0)$ comprises apart from the additive white Gaussian noise the mutual interference due to CDMA. For the results shown in Figure 7, a 3 dB higher interference level, accounting for an increased cross-correlation due to Doppler shifts, and 12 satellites in simultaneous view has been assumed. The included curves indicating the required C/N_0 for the different chipping and data rates were derived on the base of the relationship

$$C/(N_0 + I_0) = E_b/N_0 f_{\text{data}} \tag{4}$$

with f_{data} denoting the data rate and a fixed $E_b/N_0 = 12.5$ dB. The 12.5 dB are approximately required to achieve a BER of 10^{-6}, in the case of a rate $r = 1/2$, $v = 6$ convolutional encoded data transmission without satellite path diversity over a Ricean fading channel with a carrier-to-multipath-power ratio $C/M = 7$ dB and a slowly moving receiver.

As a design 'rule of thumb', it has been assumed that the CDMA self-noise should generate a total $(N_0 + I_0)$ PSD rise over the AWGN PSD level N_0 not greater than 3 dB. By a further

[¶] Path diversity is a *natural* by-product for one-way navigation system requiring by definition several satellite in simultaneous visibility. The main path diversity constraint is related to the fact that the messages broadcasted have to be the same for all satellites.

[‖] According to Reference [4] the SRC timing jitter is lower than the one computed according to Equation (3).

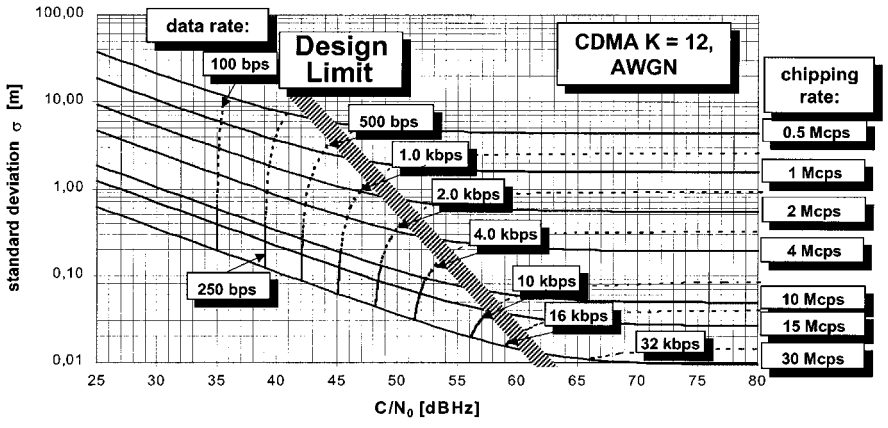

Figure 7. Relationship between data rate and accuracy.

increase of the C/N_0 beyond the 'design limit', the gain in terms of chip timing accuracy rapidly becomes negligible.

As can be seen from Figure 7, a given chipping rate and receiver C/N_0 leads to a corresponding chip timing accuracy and maximum data rate. Hence, for a chipping rate $f_C = 3$ Mcps and $C/N_0 = 45$ dB Hz the timing standard deviation is about 0.5 m, a data rate of up to 1.5 kbps can be transmitted in this case. The application of 2-fold satellite path diversity permits the doubling of the maximum bit rate or equivalently, to reduce the C/N_0 requirement for data transmission by a factor of 2.

From the results, it clearly follows that the L-band signal used for one-way accurate ranging measurement ($\sigma_R < 1$ m) can also provide a medium rate data broadcasting capability *up to thirty-times* the present GPS message data rate. The higher transmission rate can be very useful to reduce the receiver time-to-first fix (TTFF) but also to broadcast extended navigation data including more accurate ionospherical models and low-delay integrity information. Moreover, capacity for additional services using the positioning and timing as basis (e.g. broadcast service for traffic guidance, weather maps) can be offered.

3.6. Data message format

3.6.1. Basic requirements. It has been considered advantageous to split the satellite message in two parts: Basic navigation data (B-data) and Enhanced navigation data (E-data). *B-data* provides only the ephemeris, clock, ionosphere and almanac data, as well as integrity data for satellites which are close-by the satellite being tracked (i.e. the satellites that are likely to be seen by the same receiver). This integrity data does not satisfy the most stringent time-to-alarm requirements, but suffices for the low-end single-frequency Galileo receivers. In order to allow a high repetition rate of B-data message, the overall frame for B-data contains a small number of bits. Since the B-data stream is satellite unique and no diversity reception is possible, reasonably link conditions are needed.

E-data contains the complete system information (i.e. the ephemeris, clock, ionosphere and almanac data, and integrity data for all satellites). For acquisition speed-up purposes, the

information in B-data and E-data are sent in a different order, even complementary, if possible. Because the data is satellite common and diversity reception is possible, worse link conditions can be tolerated and the data can be collected from different satellites. This E-data robustness achieved through simultaneous satellite broadcasting allows among others a reliable integrity dissemination to navigation receivers.

At one carrier frequency B- and E-data are time multiplexed into the *E-NAV* data stream and transmitted with a total rate of $\approx$750 bps. At a second carrier frequency E-data type only** is transmitted on the *E-NAV′* data stream with a rate of $\approx$1500 bps. Both messages adopt a frame length of 1 s. Typically, B-data is used for initial signal acquisition while E-data is exploited under steady-state receiver conditions.

3.6.2. Frame structure. All data streams are enconded with a convolutional code with rate $r = \frac{1}{2}$ and memory $v = 6$. A CRC check code is added for frame error detection. The information and tail bits are block interleaved prior to the encoding.

The data in the *E-NAV* frame is separated into two parts. The first part is satellite unique and contains B-data. The second part is common for all satellites (E-data) and allows the use of diversity reception. Each part contains its own tail bits to allow the required separate decoding. The parameters in Table II have been preliminary selected.

After encoding and insertion of the unique word (UW) one gets 1500 bit/frame. The overall information bit rate including CRC bits is 338 bps for B-data and 394 bps for E-data. The UW is also used for solving the satellite differential delay ambiguity. This is required for E-NAV rake fingers baseband signal alignment prior to combining.

E-NAV′ contains data common for all satellites (type E-data) and uses the structure described in Table III. After encoding and insertion of UW we get 3000 bit/frame. The overall information bit rate including CRC bits is 1488 bps. The UW is again foreseen to resolve the satellite differential delay ambiguity.

3.6.3. Message content. In Reference [8] a mostly fixed schedule of message broadcasting similar to GPS was preliminary adopted. Only for urgent alarm messages (e.g. integrity failures) a change of the message order has been foreseen. This approach needs to be pursued, in order to gain more flexibility for the data transmission scheme. A flexible message scheme like the one applied to WAAS, seems more appropriate to match a second-generation system requirements. Each frame contains a header, characterising the content of the frame, and the 'payload' itself. The flexible message approach is felt best suited to accommodate the evolving Galileo applications needs. Provisions have to also be made to make the corresponding up-link facilities from the ground stations to the satellites available. It should be noted that the quasi-real-time information like integrity, can be up-linked on a (multi)-regional basis.

3.7. Overall signal structure

According to the frequency plan (refer to Section 3.1), the parameters of the overall signal structure for the three different options are summarized in Table IV.

** The E-data content is typically different at different carrier frequencies.

Table II. E-NAV frame structure (750 bits before encoding with convolutional code).

$\frac{1}{2}$ Unique word[†]	B-data and CRC Bits	Tail bits	E-data and CRC bits	Tail bits
6	338 (without diversity)	6	394 (with diversity)	6

[†] The unique word is added after encoding with the convolutional code and has in this case a length of 12. It is taken into account with half of its length in this table to show the relationship between the different parts of the frame before encoding with the convolutional code.

Table III. E-NAV′ frame structure (only E-data, 1500 bits before encoding with convolutional code).

$\frac{1}{2}$ Unique word	E-data and CRC bits	Tail bits
6	1488 (with diversity)	6

Table IV. Signal parameters for different options.

	Target C/N_0 (dBHz)	EIRP (dBW)	Carrier Freq. (MHz)	Chip rate (Mcps)	Data Stream	Info. Bit rate (bps)	FEC code rate (coded data rate (bps)	Code length (Gold seq.) (chips)	Code duration (μs)
Baseline									
E1	45	31.0	1589.742	3.069	E-NAV′	1500	$\frac{1}{2}$ (3000)	1023	333,3
E2	45	30.8	1561.098	3.069	E-NAV′	1500	$\frac{1}{2}$ (3000)	1023	333,3
E4	45	28.4	1256.244	3.069	E-NAV	750	$\frac{1}{2}$ (1500)	1023	333,3
Option 1									
G1	45	31.0	1598.949	15.345	E-NAV′	1500	$\frac{1}{2}$ (3000)	1023	66,7
E2	45	30.3	1561.098	3.069	E-NAV	750	$\frac{1}{2}$ (1500)	1023	333,3
G2	45	28.9	1589.106	15.345	E-NAV′	1500	$\frac{1}{2}$ (3000)	1023	66,7
Option 2									
E1	45	31.0	1589.742	3.069	E-NAV′	1500	$\frac{1}{2}$ (3000)	1023	333,3
E4	45	28.4	1256.244	3.069	E-NAV	750	$\frac{1}{2}$ (1500)	1023	333,3
C	38	34.0	5014.746	15.345	E-NAV′	1500	$\frac{1}{2}$ (3000)	1023	66,7

For all signals, the use of SRC-QPN with a roll-off factor $\beta = 0.2$ is proposed. In Reference [2] system link budgets for all options have been computed, in Table IV only the required satellite EIRP is incorporated.

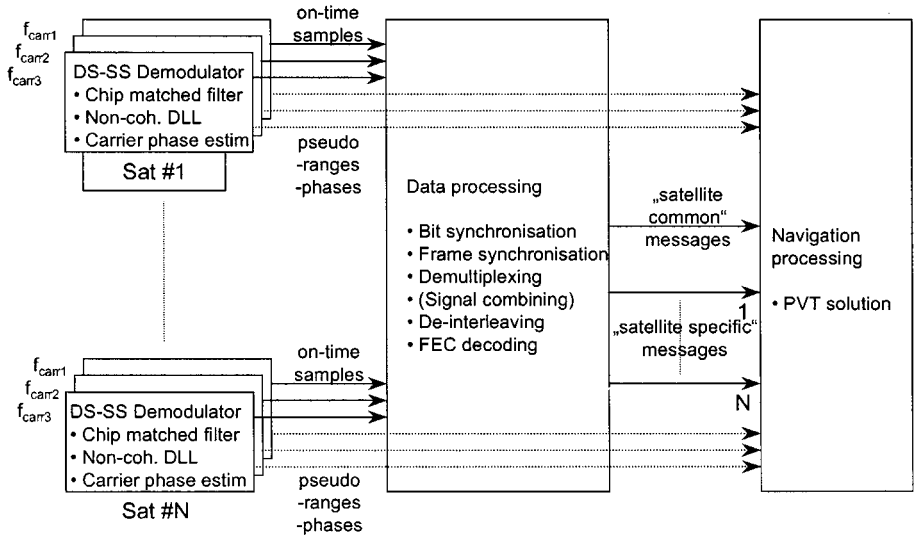

Figure 8. Overall receiver block diagram.

4. RECEIVER BLOCK DIAGRAM

4.1. Overall receiver block diagram,

Figure 8 shows a high-level block diagram of the intended receiver structure. It comprises three main sections. The *single DS-SS demodulator* includes the algorithms to determine the pseudo-ranges (DLL) and pseudo-phases (PLL). At maximum, three demodulators are required to process the signals from one satellite. Each demodulator delivers the measured pseudo-ranges and -phases to the navigation processing block and the de-spread on-time signal samples to the data processing block. The *data processing block* extracts for each received signal the corresponding bit/data frame timing and the message bits. Details are explained in Section 4.3. The *navigation processing block* processes the extracted pseudo-ranges, -phases and messages in order to derive a solution for the position, time, and velocity.

A simpler approach for the receiver structure, compared with Figure 8, would only exploit one carrier per satellite resulting in a need for ionospherical correction data, restricted access to transmitted navigation data, and difficulties for a successful carrier phase ambiguity resolution. Exploiting at least two carriers allows ionospherical correction and faster access to more navigation data, while the access of three carriers supports the application of TCAR techniques for carrier phase ambiguity resolution [8]. Note that initial signal acquisition can be based on fast search engines as currently employed for CDMA wireless networks hand-held terminals.

4.2. Demodulator finger

A block diagram for a possible non-coherent DLL structure can be found in Reference [4]. It comprises an analogue chip matched filter for the incoming signal with subsequent digitalisation.

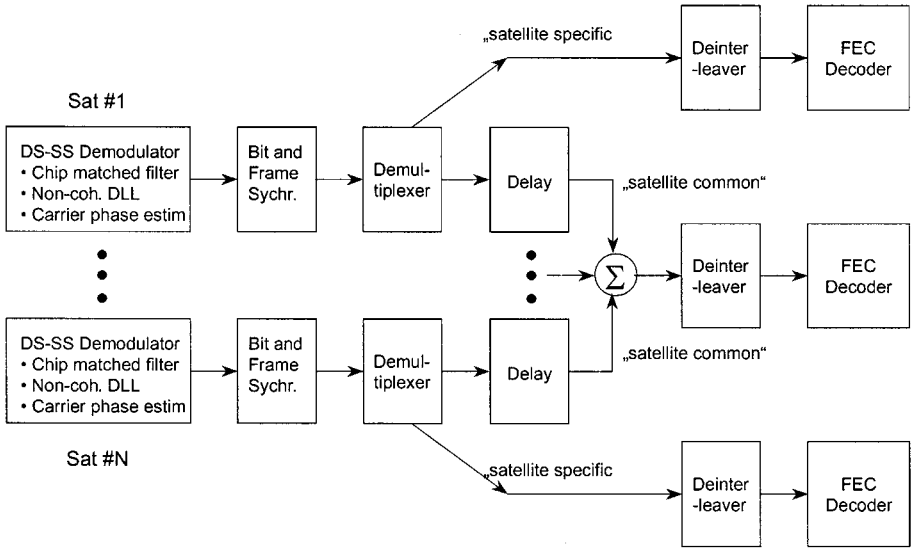

Figure 9. Receiver block diagram for data reception.

For a standard early–late spacing of T_C two samples per chip are required at the CMF filter output. As already mentioned, asynchronous sampling is easily feasible due to the application of interpolation. The correlation process is executed in the digital domain, as well as the loop filtering and the generation of the reference signals. For the carrier phase tracking the well known Costas loop can be applied [9].

4.3. Data transmission and decoding strategy

As previously discussed, the data transmission follows a two-fold strategy. Each satellite transmits 'satellite specific' and 'satellite common' information. The 'satellite specific' part has to be extracted from the data stream of each satellite. As can be seen from Figure 9, the on-time output of the signal DS-SS demodulator feeds a synchroniser block, which extracts the correct symbol timing and by searching for a frame synchronisation word ('unique word') the frame timing as well. The subsequent de-multiplexer can filter the 'satellite specific' part. The extracted signal samples are de-interleaved and subsequently fed into the FEC decoder in order to determine the transmitted information bits.

In order to extract the 'satellite common' part, the bit- and frame synchronization has to be established for each demodulator satellite finger separately. Then the de-multiplexer block can extract the corresponding 'satellite common' signal samples. Due to the different distances between the user terminals and the satellites corresponding data frames arrive at the receiver at different times. To compensate for the differential finger delays (of up to 20 ms) before combining the signal samples, they are stored in a buffer. Since the frame synchronization is established at this stage, the differential delay can be easily determined, thus, the signal samples coherently

Table V. L-band channel parameters.

Scenario	C/M (direct path) (dB)	Doppler bandwidth (Hz)	Number of echoes	Delay (ns)	Relative power (dB)	Doppler bandwidth (Hz)	C/M (total) (dB)
En-route	15	1	1	50	− 3†	1	3.0
Final approach	10	1	1	44	− 6	420	4.7
Urban car	7	70	4	60	− 27	70	6.8
				100	− 27	70	
				130	− 27	70	
				250	− 27	70	
Urban ped.	7	4	4	60	− 27	4	6.8
				100	− 27	4	
				130	− 27	4	
				250	− 27	4	
Rural	6	140	2	100	− 28	140	5.9
				250	− 31	140	

† It should be noted that having an echo, which is only 3 bB lower than the direct path, represents a type of worst case assumption.

accumulated. The resulting sample stream is de-interleaved and fed into the FEC decoder. This E-data processing is akin to a rake demodulator.

5. PERFORMANCE RESULTS

5.1. Channel models

The performance of the signal design in an additive white Gaussian noise (AWGN) as well as different multipath/fading channels has been studied. In the case of multipath/fading, five operational scenarios have been identified and the corresponding channel models developed: en-route aeronautical channel, final approach aeronautical channel, urban pedestrian, urban car and rural environment. For the realization of the channel models a tap-delay line approach, each tap representing a group of received signal components that cannot be further distinguished, has been applied.

The first tap is characterized by a Rician amplitude distribution (includes the direct path and a diffuse component) with a Rice factor C/M and a rectangular-shaped Doppler power spectrum with a maximum Doppler frequency $f_{\mathrm{DMax}} = (v/c)\, f_{\mathrm{carr}}$ (v is the speed of mobile, c the speed of light, f_{carr} the carrier frequency).

The other taps, representing the echo components, are characterized by a Rayleigh amplitude distribution, a rectangular-shaped Doppler power spectrum with a maximum Doppler frequency f_{DMax}, and a certain relative delay with respect to the first tap. Table V summarizes the parameters of the considered channel models [2].

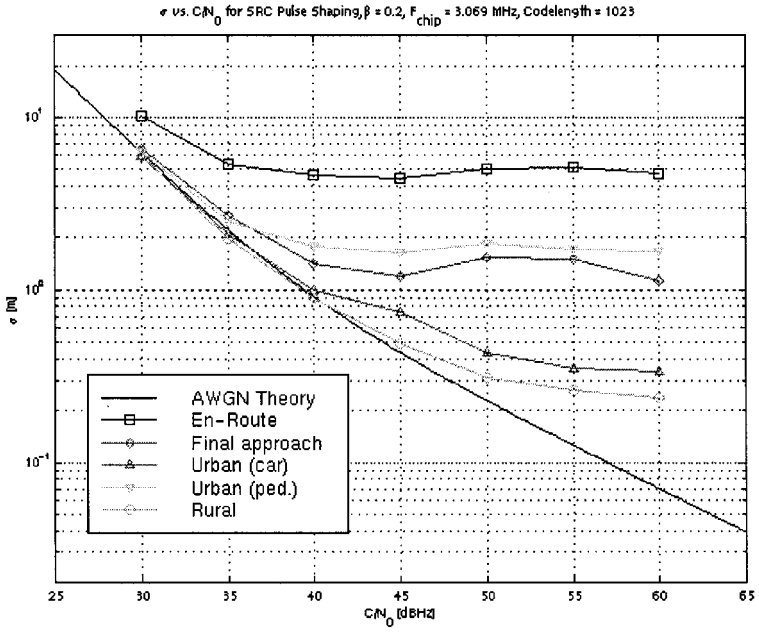

Figure 10. Code phase jitter for QPN B in multipath/fading environment.

5.2. Results for the AWGN channel

Referring to Figure 7 in Section 4.5, we can conclude (a) for a chipping rate of $f_c = 3.069$ Mcps, a RMS code phase jitter of $\sigma \approx 0.5$ m is achieved at $C/N_0 = 45$ dB Hz (data rate $f_{\text{data}} < 1500$ bps); (b) that is case of two-fold diversity a BER of 10^{-6} can be reached at approximately $C/N_0 = 42$ dB Hz, but the code phase jitter is increased to $\sigma \approx 0.7$ m; (c) for a chipping rate of $f_c = 15.345$ Mcps, a RMS code phase jitter of $\sigma \approx 0.1$ m is achieved at $C/N_0 = 45$ dB Hz (data rate $f_{\text{data}} < 1500$ bps).

5.3. Results for multipath/fading channels

The signal structure described in Section 4.3.1. has been used for the following simulations with a chip rate $f_C = 3.069$ Mcps and a roll-off $\beta = 0.2$. The receiver structure included a non-coherent DLL (loop bandwidth 2 Hz, early–late spacing T_c, pre-detection bandwidth 3000 Hz) and a BPSK Costas loop (loop bandwidth 20 Hz, symbol rate: 3000 Hz).The other satellites CDMA interference was included in the AWGN noise power level.

5.3.1. Code phase tracking. The performance of code phase jitter as shown in Figure 10 improves with the scenario order (see): en-route aeronautical, urban pedestrian, final approach aeronautical, urban car, and rural. For all channel types and RMS the code phase jitter 'floor' can be observed with increasing C/N_0. This is caused by the fading processes of the echoes

which result[††] in a time-varying loop S-curve zero crossing point. Depending on the channel model, above a certain C/N_0, the impact of zero-crossing variations dominates the AWGN jitter contribution.

As can be concluded from Figure 10, the worst performance is obtained for the 'en-route aeronautical' channel type. This is caused by the combination of two effects: for this channel, both diffuse components (direct path and echo) have a very low Doppler bandwidth (1 Hz) and a relatively high power in the echo. With a loop bandwidth of 2 Hz the non-coherent DLL is able to track the combination of direct path and the diffuse components. Due to the fact that the presence of an echo causes a slow varying bias for the loop-S curve zero-crossing point, a large variation of the resulting measured code phase ($\sigma \approx 5$ m) is observed. For the final approach aeronautical channel, the situation is improved mainly since the Doppler bandwidth of the echo is very high (420 Hz). Therefore, the non-coherent DLL is not able to track the variations caused by the echo. The urban pedestrian channel is affected by the number of echoes and their relative large relative delay (up to 250 ns = 75 m). According to the multipath envelope considerations reported in Reference [10], the maximum impact of an echo occurs for delays between 50 and 75 m for the 3.069 Mcps signal. Again the effect is magnified by the small Doppler bandwidth of 4 Hz. The code phase jitter performance is further improved for Urban car and Rural channel due to the low multipath power and high Doppler bandwidth of 70, 140 Hz, respectively.

Concerning the results for higher chipping rates ($f_C = 15.345$ Mcps) it turned out, that for urban pedestrian, urban car, and rural channels a considerable improvement could be achieved while for the en-route aeronautical and final approach aeronautical channel no significant difference compared to $f_C = 3.069$ Mcps has been observed. The main reason for this observation is due to the relative delays of the echoes. Echoes having a delay greater than 1.5 chip duration (≈ 100 ns at $f_C = 15.345$ Mcps) are suppressed and, hence, do not have an degrading effect on the code phase jitter.

5.3.2. Carrier phase tracking. It should be noted that the presented carrier phase error has been determined with respect to the phase of the direct path (assumed to be zero). For other application areas such as communications the phase error is measured with respect to the phase of the sum of the direct path and its diffuse component. This reflects the fact that for symbol or bit detection it is preferable to gather as much energy as possible even including the diffuse components.

The results for the carrier phase jitter are depicted in Figure 11. The performance of carrier phase jitter improved with the same scenario order as the code phase jitter previously discussed. The worst performance corresponds to en-route aeronautical channel and its caused by a small delay strong echo combined with a very low Doppler bandwith. The bad performance of urban pedestrian is caused by the larger power of the diffuse component affecting the zero delay direct path. A slightly better performance has been found for the final approach aeronautical channel due to a smaller power of the diffuse component. The impact of the echo is very small due to the high Doppler bandwidth. Urban car and rural channels exhibit an even better performance because of the high multipath Doppler bandwidth. Similar to the code phase, for all channel types

[††] In particular for slow fading channels.

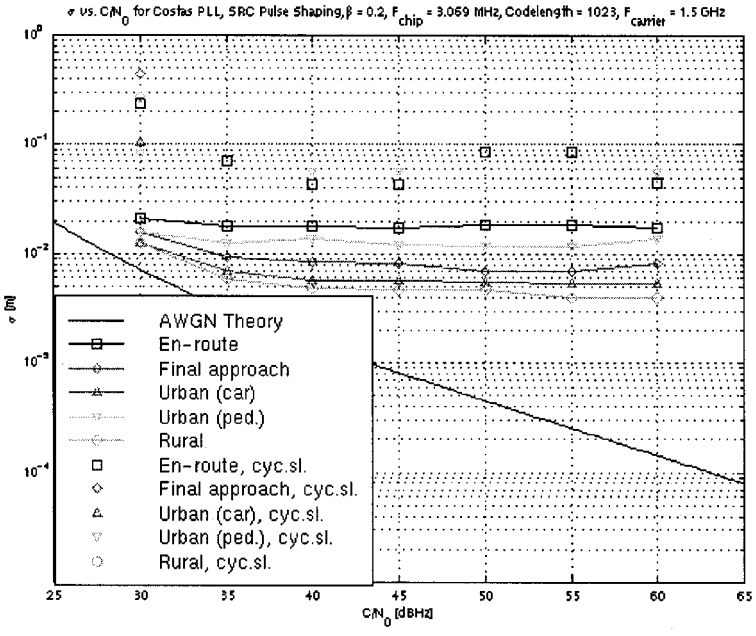

Figure 11. Carrier phase jitter for QPN B in multipath/fading environment.

Table VI. C/N_0 and E_b/N_0 values required to reach a BER for E-NAV/B-data and E-NAV/E-data.

En-route aeronautical	C/N_0 (dB Hz)	E_b/N_0 (dB)
E-NAV/B-data	> 50	> 21
E-NAV/E-data (3-fold diversity)	> 43	> 14
Urban car	C/N_0 (*dB Hz*)	E_b/N_0 (dB)
E-NAV/B-data	> 39	> 10
E-NAV/E-data (3-fold diversity)	> 38	> 9

a carrier phase jitter 'floor' can be observed with increasing C/N_0, due to echoes resulting in a time-varying tracking point even in the absence of noise.

Since cycles slips occurred in some simulation runs, the carrier phase error has been re-mapped into the interval $[-\pi/2, \pi/2]$. The point in Figure 11, which are connected by a line, include the mapping, while the points alone represent the resulting raw jitter. Increased carrier phase cycle slip rates have been observed for channels with a high carrier phase jitter floor such as en-route aeronautical and urban pedestrian.

5.3.3. Bit/frame error rate. Table VI summarizes simulation results for the required C/N_0 and E_b/N_0 values, respectively, required to achieve a bit error rate BER $= 10^{-6}$ for two different multipath/fading channels. More results are reported in Reference [2].

From Table VI it can be seen that the application of diversity reception results in terms of total[‡‡] C/N_0, in a gain of about 7 dB for the en-route slowly varying aeronautical channel. In a faster fading channel the potential gain due to 3-fold diversity is reduced to 1 dB. It might be noted, that for the En-route aeronautical channel and E-NAV/B-data transmission the target BER cannot be met for $C/N_0 = 45$ dB Hz.

6. SUMMARY AND CONCLUSIONS

The design drivers for a second-generation satellite navigation system signal have been illustrated together with the main design parameter trade-offs. Exploiting modern digital signal processing techniques, the required ranging accuracy can be achieved with a modest L-band bandwidth occupation and an affordable payload EIRP in the order of 31 dB W for MEO orbits. It has been shown, how the adoption of a square-root raised-cosine chip shaping allows to maximize the ranging accuracy for a given bandwidth and to reduce measurement sensitivity to the multi-path. A 15-fold (resp. 30-fold) increase in the navigation signal broadcasting capabilities will make possible to greatly reduce the time-to-first-fix, significantly increases the data refreshing rate, thus considerably enhancing the integrity functionality and provide auxiliary information that can further improve the system accuracy and integrity. Moreover, by exploiting satellite path diversity the reliability of common network broadcast information including integrity is largely increased. Very high-accuracy positioning can be eventually provided through widelaning technques [8] requiring simultaneous demodulation of the navigation signal broad-casted at three different carrier frequencies. Although attractive in principle, the combined use of L and C-band appears less appealing as for omini-directional user antennas the re-quired C-band EIRP ($\approx$40 dB W) exceeds current technological limits even for data rates of 1500 bps, although exploiting diversity (fourth order) can help to reduce the required EIRP by up to 6 dB to 34 dB W. Another drawback can be seen in the need of two front-ends due to the large frequency difference between L- and C-band. The signal design performance has been validated through extensive computer simulations for the most representative operational scenarios.

REFERENCES

1. European Commission Communication. Galileo — Involving Europe in a New Generation of Satellite Navigation Services. Brussels, February 1999.
2. Schweikert R, Woerz T. Signal design and transmission performance study for GNSS-2. *Final Report*, Document No SDS-REP-DLR/NT-02/99, ESA Ref. 12182/96/NL/JSC, October 1998.
3. Parkinson BW, Spilker JJ. GPS: theory and applications volume I. *Progress in Astronautics and Aeronautics*, 1996; 163.
4. de Gaudenzi R, Luise M, Viola R. A digital chip timing recovery loop for band-limited direct-sequence spread-spectrum signals. *Transactions on communications* 1993; 45 (11): 1760–1769.
5. van Nee R. Multipath and multi-transmitter interference in spread-spectrum communication and navigation systems. *Ph.D. Thesis*, Technical University of Delft, May 1995.
6. Lawrence Weill. C/A code pseudoranging accuracy — how good can it get? *ION GPS*-94, Salt Lake City, 1994; 133–141, 20–23 September 1994.

[‡‡] Aggregate C/N_0 for all satellites used for diversity.

7. Garin L, Rousseau J-M. Enhanced strobe correlator multipath rejection for code and carrier, *ION* 97, Kansas City, 1997; 559–568, 16–19 September 1997.
8. Spectra Precision TERRASAT and Socratec GmbH. Study on precise relative position using GNSS-2 TCAR. ESA Ref. 12406/97/NL/DS.
9. Mengali U, D'Andrea A. *Synchronisation Techniques for Digital Receivers*. Plenum Press: New York and London, 1997, ISBN 0-306-45725-3.
10. Woerz T. Technical note on multipath envelope. Document No. NAFEX-TN-DLR/NT-02/98, NAFEX Phase 2, ESA Ref. 12292/97/NL/JSC, June 1998.

AUTHORS' BIOGRAPHIES

Robert Schweikert received his Diploma degree in 1977 and his Doctoral degree in 1983 from the University of Frankfurt. Since 1978 he was with the German Aerospace Center where he became in 1985 Head of the Communication Systems group and in 1993 Head of the Communications Theory department. In 1991/1992 he was assigned to Intelsat, Washington, DC. In December 1998, he left the German Aerospace Center and is presently with AUDENS ACT Consulting GmbH, which he co-founded in 1998. In his function as department head, he has been responsible for numerous telecommunication contracts, in particular, in the area of satellite communications and, more recently, also in the field of satellite navigation. So, he has been project manager of the 'Signal Design and Transmission Performance Study for GNSS2', sponsored by the European Space Agency (ESA).

Thomas Wörz was born in Stuttgart, Germany, in 1961. He received the Dipl.-Ing. degree in electrical engineering from the Technical University of Stuttgart, Germany, in 1988 and his Ph.D. from the Technical University of Munich in 1995. Since 1988 he has been with the Institute of Communications Technology of the German Aerospace Center (DLR), Oberpfaffenhofen. In 1991 he spent a three-month period as a guest scientist at the Communications Research Center (CRC), Ottawa. In 1999 he co-founded the AUDENS Advanced Communications Technology Consulting GmbH and works as a technical consultant to industry and agencies. His research interests include channel coding, coded modulation, synchronisation, signal processing, and system design. Currently, he is involved in the definition of the Galileo European Navigation system.

Riccardo De Gaudenzi was born in Italy in 1960. He received the Doctor Engineer degree (cum Laude) in electronic engineering from the University of Pisa, Italy in 1985. From 1986 to 1988 he was with the European Space Agency (ESA), Stations and Communications Engineering Department, Darmstadt (Germany) where he was involved in satellite telecommunication ground systems design and testing. In particular he followed the development of two new ESA's satellite tracking systems. In 1988 he joined the ESA's Research and Technology Centre (ESTEC), Noordwijk, The Netherlands where he is holding a position as senior telecommunication engineer in the Electrical Systems Department. He is responsible for the definition and development of advanced satellite communication systems for fixed and mobile applications. He is also involved in the definition of the Galileo European Navigation System. In 1996 he spent one year with Qualcomm Inc., San Diego USA, in the Globalstar LEO project system group under an ESA fellowship. His current interest is mainly related with efficient digital modulation and access techniques for fixed and mobile satellite services, sychronization topics, adaptive interference mitigation techniques and communication systems simulation techniques.

Alexander Steingass was born in Mettmann, Germany, in 1969. He studied electrical engineering from 1989 to 1996 at the University of Ulm, Germany. In 1996 he received a Dipl. -Ing. degree in electrical engineering working in his Diploma thesis on a new frame synchronisation approach. Since January 1997 he has been working as a research staff member at the Institute for Communications Technology of the German Aerospace Center (DLR). He has designed the software architecture for a signal simulator for a second generation satellite navigation system (Galileo) in national and European projects.

Armin Dammann was born in Laupheim, Germany, in 1969. He studied electrical engineering from 1991 to 1997 at the University of Ulm, Germany. In 1997 he received a Dipl.-Ing. degree in electrical engineering. Since October 1997 he has been working as a research staff member at the Institute for Communications Technology of the German Aerospace Center (DLR). His current research interests and topics of work include synchronisation in CDMA systems for navigation purposes, Data Link Layer (OSI Layer 2) simulations for future aeronautical communications systems and soft decision decoding of generalized concatenated codes.